N-heterocycle-containing sulfonamides as potential inhibitors of the cancer-related Vps34 enzyme: A theoretical study

Man Nguyen An Khanh, Le Minh Duc, Dang Thanh Tuan, Pham Anh Son, Do Huy Hoang, Nguyen Van Ha*

University of Science, Vietnam National University - Hanoi, 334 Nguyen Trai Street, Thanh Xuan Ward, Hanoi, Vietnam

Received 4 August 2025; revised 27 October 2025; accepted 16 November 2025

Abstract:

This work provides a theoretical assessment of 30 N-heterocycle-bearing sulfonamide derivatives as prospective inhibitors of the cancer-associated enzyme Vps34, a central regulator of autophagy and tumour development. Molecular docking simulations carried out with AutoDock Vina ranked the compounds by binding affinity, grouping them into weak, moderate, and strong binders. Six derivatives (8, 12, 13, 14, 18, 30) displayed the most favourable interactions with key active-site residues such as phenylalanine PHE612, isoleucine ILE634, tyrosine TYR670, leucine LEU750, ILE760, lysine LYS636. These leading candidates were subsequently evaluated for drug-likeness using Lipinski's Rule of Five and oral bioavailability via SwissADME radar plots, all of which indicated suitable profiles. Complementary ADMET predictions from Deep-PK supported acceptable pharmacokinetic behaviour and manageable safety risks. Furthermore, molecular dynamics simulation were also carried out to gain insights into the interactions between Vps34 and compound 30. Throughout the studies, compound 30 emerged as the most promising lead, combining strong binding affinity with favourable physicochemical features, high predicted oral bioavailability, and favourable protein interaction profile. Accordingly, additional *in vitro* and *in vivo* investigations are needed to fully establish the therapeutic potential of sulfonamide scaffolds, especially compound 30, as Vps34-targeted anticancer agents.

Keywords: **anticancer, molecular docking, molecular dynamics, N-heterocycle, sulfonamide, Vps34.**

Classification numbers: **2.2, 3.3**

1. Introduction

Vps34 is the sole class III enzyme within the phosphoinositide 3-kinase (PI3K) family in humans. Its primary role is to generate phosphatidylinositol 3-phosphate (PI(3)P), a crucial lipid that supports numerous cellular activities, such as autophagy regulation, management of endocytic vesicle transport, and preservation of cellular equilibrium. Multiple sources highlight that Vps34 expression correlates with tumorigenic activity in human cancer cells [1-4]. It has also been demonstrated that Vps34 activity can modulate immune responses within tumours, aiding in the suppression of anti-tumour immunity [5]. These findings have galvanised interest in therapeutically targeting Vps34, and a variety of chemotypes have been pursued as inhibitors, including morpholine-bearing dihydropyrazolopyrazinones, piperazinone derivatives, indole alkaloids, and pyrazolo[1,5-a] pyrazinones [6].

Sulfonamides are a class of synthetic compounds characterised by the presence of the sulfonamide functional group, which forms the basis for several important drug classes. These compounds were among the first effective systemic antibacterial agents, revolutionising the treatment of infectious diseases. Sulfonamides are used to treat a variety of bacterial infections, including urinary tract infections, respiratory tract infections, and certain types of meningitis [7]. Several sulfonamide compounds have been approved by the Food and Drug Administration (FDA) as commercial drugs. Examples include celecoxib (a COX-2 inhibitor for pain and inflammation), thiazide and loop diuretics (e.g., hydrochlorothiazide, furosemide) for hypertension and oedema, sulfonylureas (e.g., glipizide, glyburide) for type 2 diabetes, and topical agents such as silver sulfadiazine and mafenide for burn treatment (Fig. 1).

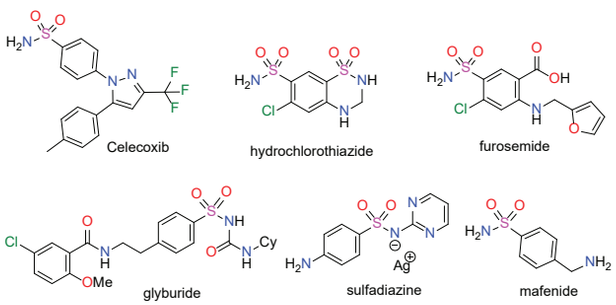

Fig. 1. Structures of FDA-approved drugs containing sulfonamide core.

Recent studies highlight the rising anticancer potential of sulfonamide derivatives across multiple mechanisms. These compounds function as inhibitors of essential

*Corresponding author: Email: hanv@hus.edu.vn

CC BY NC ND
Crossref Similarity Check Powered by iThenticate

protein, disrupting cancer cell metabolism, signalling, invasion, and epigenetic regulation [8]. Notably, tailored coumarin-sulfonamides have shown strong inhibition of CA IX in lung and breast cancer cells, reducing proliferation and invasiveness [9]. Sulfonamide derivatives bearing coumarin and benzodiazepine exhibit significant antiproliferative effects, occasionally outperforming celecoxib *in vitro* [10]. It has also been demonstrated that a coumarin-functionalised sulfonamide derivative can activate PKM2 and induce apoptosis in lung cancer cells [10]. Overall, the versatility of the sulfonamide scaffold provides an excellent platform for exploring new promising candidates for anticancer drug development.

In this work, we focus on theoretically exploring the potential use of several reported N-heterocycle-bearing sulfonamides as inhibitors of Vps34 enzyme. Their pharmacophore kinetics of the sulfonamide derivatives are also examined.

2. Materials and methods

2.1. Molecular docking

Protein structural validation: The structure of the Vps34 protein (ID: 4uwh) was retrieved from the Protein Data Bank [11]. Its structure contained a crystallised tetrahydro-4H-pyrimido[1,2-a]pyrimidin-4-one ligand (Fig. 2).

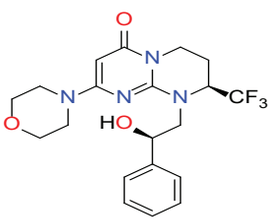

Fig. 2. Structure of the tetrahydro-4H-pyrimido[1,2-a]pyrimidin-4-one crystalised with the protein.

The protein data bank file of the Vps34 protein, or its PDB ID, was utilised for validation using multiple web-based tools. Utilising the UCLA-DOE IGP Service, ERRAT [12] gave an overall quality factor of 97.05%, while VERIFY3D [13] showed 83.39% of the residues with an averaged 3D-1D score≥0.1. A 93.6% favoured region and 6.4% allowed region were obtained from PROCHECK analysis [14] through PDBSum [15]. Additionally, the Ramachandran plot (Fig. 3) obtained from the SWISS-MODEL Structure Assessment [16], based on MolProbity [17], confirmed 99.45% residues in Ramachandran favoured regions (Fig. 3) with no outliers detected. Overall, the validation results strongly support that the Vps34 protein structural model is accurate, stereochemically valid, and suitable for further structural and functional studies.

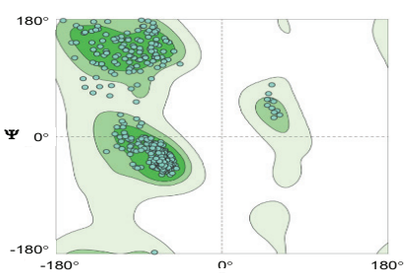

Fig. 3. Ramachandran plot of the protein obtained from the SWISS-MODEL Structure Assessment.

Preparation of protein structures: The active sites of the proteins were identified using Discovery Studio Visualiser 4.0 software [18]. Water molecules and crystallised ligands were removed, and polar hydrogen atoms were added using AutoDock Vina software. The active site positions were reset using Molecular Graphics Lab (MGL) AutoDock Tools 1.5.7 software.

The 3D structure of the ligands was constructed using GaussView software, which then underwent optimisation using Avogadro (version 1.2.0) software. The Universal Force Field (UFF) was employed since it is a molecular mechanics force field applicable to every atom of the periodic table with atomic number lower than 103 [19]. The optimised structures were then converted to .pdbqt format using AutoDock Tools 1.5.7.

Docking the ligands into the active site of the protein was performed with AutoDock Vina software using a grid box size of 40×40×40 Å, centred at (x, y, z)=(46, 92, 35). Discovery Studio Visualizer 4.0 software was utilised to observe the interactions between the protein and the ligands. The binding affinity was assessed through its interactions with amino acids in the active site and the interaction energy calculated by the scoring function of AutoDock Vina.

2.2. Evaluation of drug-likeness with Lipinski's rule of five criteria and bioavailability radar

The drug-likeness examination was evaluated taking into account molecular characters, such as molecular weight (MW), high lipophilicity (LogP), hydrogen bond donors/acceptors (HBD/HBA1), and molar refractivity (MR) in accordance with the Lipinski's rule of five. In addition, bioavailability radar was generated using physicochemical properties, including molecular size, solubility, flexibility, polarity, lipophilicity, and saturation. All their predicted parameters were obtained using SwissADME, a useful tool for theoretically supporting drug development [20-23]. The data were either used directly (as tabulated in table) or drawn in form of graph for better visualisation (bioavailability data).

2.3. In silico prediction of pharmacokinetic properties, toxicity

To evaluate the physicochemical characteristics, pharmacokinetic behaviour, and toxicity profiles of the compound, the web-based tool Deep-PK [24] was utilised. This trusted platform has recently been widely used to comprehensively analyse the ADMET profiles of the compounds [25, 26].

2.4. Molecular dynamics simulations

Molecular dynamics (MD) simulations serve as an essential tool in drug discovery and development, providing comprehensive insights into the conformational dynamics and stability of protein-ligand interactions. In this study, MD simulations were carried out to evaluate the most promising candidate - compound 30. To explore the interaction patterns between the selected compound and the Vps34 enzyme, an all-atom MD simulation was performed for 200 ns using the GROMACS 2022 software package [27]. The analysis focused on several key parameters - including hydrogen bonding (H-bonds), root mean square fluctuation (RMSF), radius of gyration (Rg), root mean square deviation (RMSD), and solvent-accessible surface area (SASA) - to elucidate the structural and dynamic characteristics of the protein-ligand complex.

3. Results and discussion

3.1. Protein selection and validation of molecular docking

Among available Vps34 crystal structures and ligand complexes, we selected the human Vps34 entry 4UWH from the Protein Data Bank [11], which contains the co-crystallised tetrahydro-4H-pyrimido[1,2-a]pyrimidin-4-one ligand. Its high resolution (1.93 Å resolution) makes it a suitable template for docking simulation. In addition, it has been demonstrated that its active site is highly conserved across multiple pathogenic fungi, supporting modelling of fungal Vps34 interactions for further experimental follow-up research [28].

To validate the docking procedure, redocking of the tetrahydro-4H-pyrimidopyrimidin ligand into the protein's active site was performed. The theoretically obtained ligand conformation (through docking) was then superimposed on the crystal structure of tetrahydro-4H-pyrimidopyrimidinl (Fig. 4).

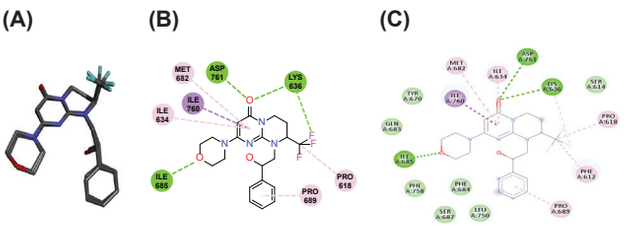

Fig. 4. Docking validation results: (A) Superimposed image of the theoretically predicted and experimentally determined structures of tetrahydro-4H-pyrimidopyrimidine; **(B)** visualisation of the ligand-protein interactions based on the docking study; **(C)** structural alignment based on the X-ray crystallographic structure.

The resulting root mean square deviation for heavy atoms was 0.32 Å, which is well below the commonly accepted threshold of 1.5-2 Å [29-31], indicating that the redocked pose closely resembles the crystallised structure.

Detailed analysis of the binding interactions revealed that the ligand forms hydrogen bonds with the protein active site, specifically between the ketone oxygen and the hydrogen atoms of aspartic acid (ASP761) and lysine (LYS636), as well as between the ether oxygen and a proton of isoleucine (ILE685). Additionally, a weaker C-H···F interaction was observed. Hydrophobic interactions, including alkyl and π-alkyl interactions, further contribute to the binding affinity. These key interactions are consistent with those observed in the co-crystallised protein-ligand complex, further validating the docking procedure used.

3.2. Collection of molecular set

A collection of 30 reported N-heterocycle-bearing sulfonamide derivatives [32-34] was selected for this study. The compounds exhibit significant variation in their N-heterocyclic cores, which extend well beyond simple pyridine rings (Fig. 5).

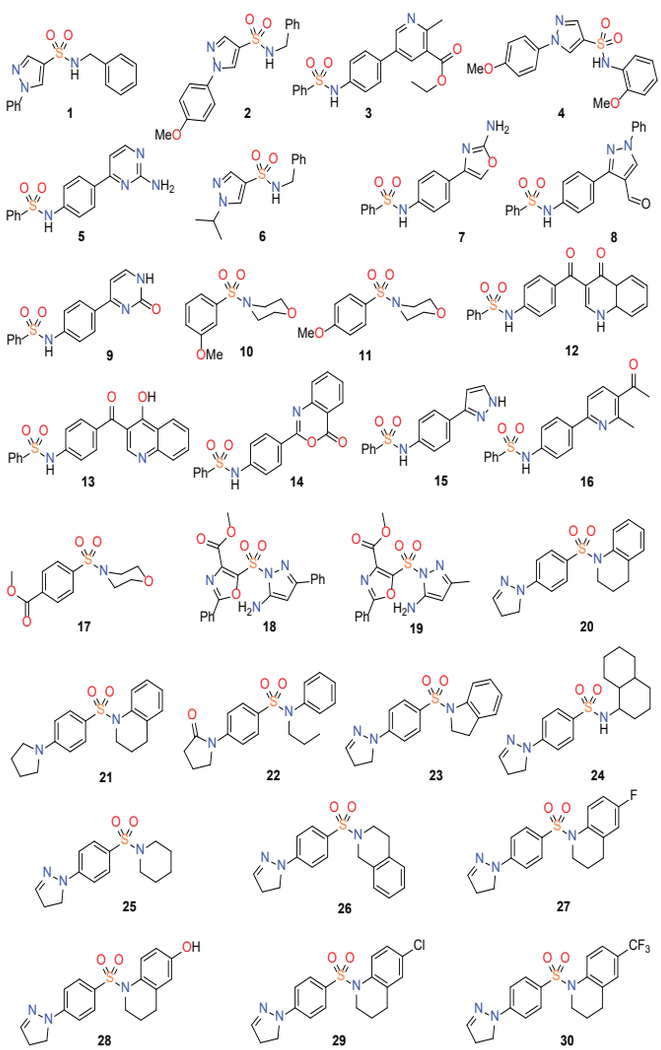

Fig. 5. Structures of the N-heterocyclic bearing sulfonamides in this study.

The heterocycles include complex fused systems, triazoles, pyrazoles, and other nitrogen-containing aromatic and non-aromatic rings, often substituted with various functional groups such as amino, methoxy, carbonyl, and fluorinated groups. This structural diversity around sulfonamide and nitrogen heterocycles is expected to enhance the likelihood of identifying promising candidates for further drug development.

3.3. Docking of the sulfonamides

After validation, docking studies were conducted with the collection of 30 N-heterocycle-bearing sulfonamides. The results were evaluated using binding energy (Table 1).

Table 1. Calculated binding energy of the compounds and the protein.

Compound	Binding energy (kcal/mol)	Compound	Binding energy (kcal/mol)
1	8.0	16	8.2
2	7.7	17	6.1
3	8.2	18	8.7
4	7.3	19	7.8
5	8.2	20	8.3
6	7.1	21	7.9
7	7.7	22	7.7
8	8.6	23	7.7
9	8.2	24	7.7
10	6.1	25	6.9
11	6.4	26	8.5
12	9.0	27	8.5
13	9.0	28	7.9
14	9.5	29	8.4
15	8.1	30	8.9

Based on the calculated binding energy data, the sulfonamide derivatives can be categorised into three groups: strong, medium, and weak interactions. The weak interaction group comprises samples with binding energy of less than 8.0 kcal/mol. This includes samples 2, 4, 6, 7, 10, 11, 17, 19, 21-25 and 28 with the weakest interaction recorded at 6.1 kcal/mol (for 10 and 17). The binding of some representative compounds, namely 2, 19, 21, and 22, is presented in Fig. 6.

These low affinities indicate that these samples may not be optimal candidates for strong binding in the studied context. This group features not only compounds with predominantly non-polar fragments (such as 6, 21, 25) but also compounds which appear to be good hydrogen-bond acceptors and donors (such as 2, 4, 7, 19, and 22, Fig. 6).

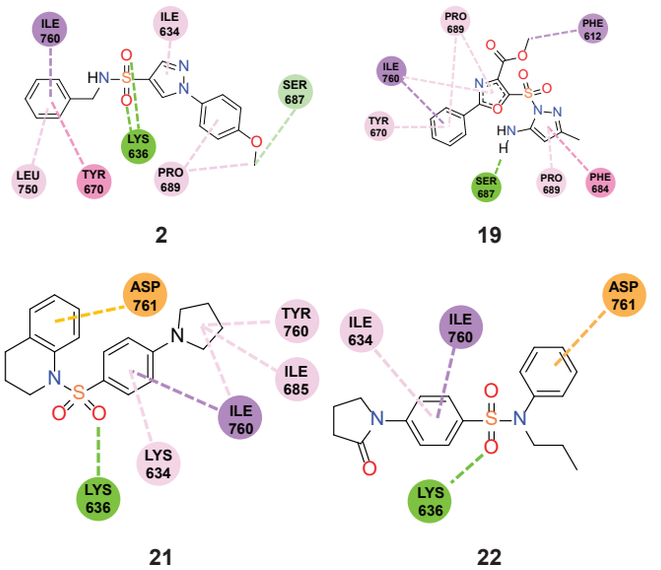

Fig. 6. Interaction of compounds 2, 19, 21, 22 with Vps34.

The second group, with binding energies ranging from 8.0 to 8.5 kcal/mol, demonstrates moderate binding affinity. This includes samples such as 1, 3, 5, 9, 15, 16, 20, 26, 27, and 29. Representative interactions are presented in Fig. 7.

Within the active site of the protein, compound 3 is anchored by a hydrogen bond with lysine (LYS613) at a distance of 2.46 Å. This interaction is reinforced by π-π stacking with phenylalanine (PHE612) and a weak C-H···O hydrogen bond involving glutamine (GLN683). Additional stabilisation arises from hydrophobic contacts, including CH-π and π-sulphur interactions, with residues such as ILE634, ILE685, PHE758, TYR670, ILE760, and PHE612. For compound 9, the binding is primarily driven by a hydrogen bond with lysine (LYS636, 2.60 Å) and a π-anion interaction with aspartic acid (ASP761) at a distance of 4.16 Å, both serving as key anchoring forces. Further stabilisation is provided by N-H···π interaction with PHE612 and hydrophobic interactions between the ligand's

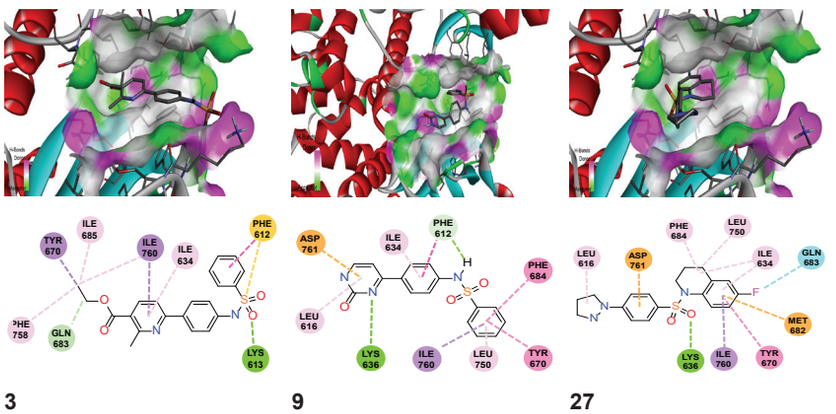

Fig. 7. Compounds 3, 9, and 27 in the protein active site and the respective interaction between the compound and protein.

aromatic moiety and residues ILE634, ILE760, TYR670, LEU750 and PHE684. In the case of compound 27, the ligand is chiefly stabilised by a hydrogen bond with Lysine (LYS636) at a distance of 2.21 Å, and a fluorine-carbonyl interaction involving GLN683 at a distance of 3.45 Å. This is complemented by a network of interactions including π-anion (ASP761), π-sulphur (MET682), and π-π stacking (TYR670). Additional, though less prominent, hydrophobic contacts are observed with LEU616, PHE684, LEU750, ILE634, and ILE760.

The strong interaction group includes compounds with binding energies higher than 8.5 kcal/mol, indicating high binding affinity. This group includes compounds 8, 12, 13, 14, 18, and 30. Notably, several compounds in this group show exceptionally high binding energies, reaching as high as 9.5 kcal/mol, suggesting strong interaction. The visualisation of these molecules within the protein active site and their interactions is presented in Fig. 8.

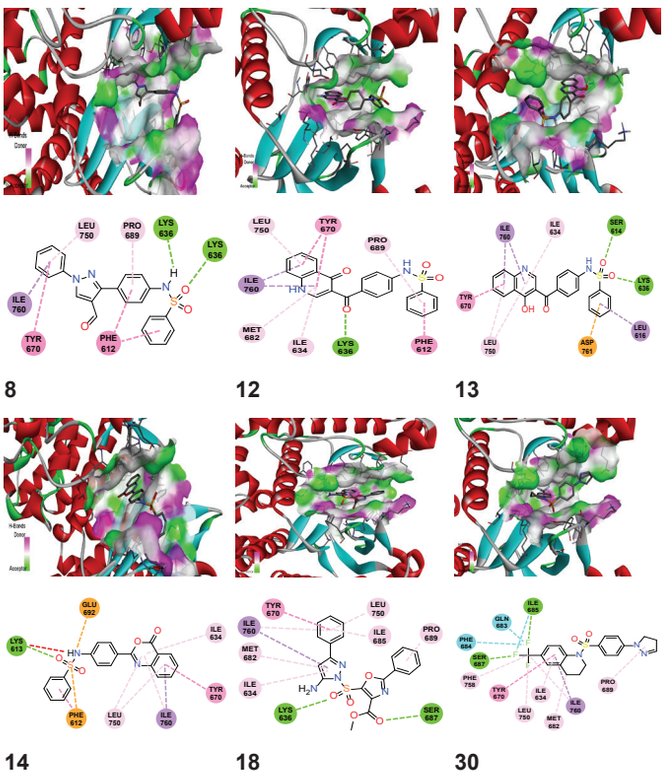

Fig. 8. Compound 8, 12, 13, 14, 18 and 30 in the protein's active site and the respective interaction between the compound and protein.

It can be observed that compound 8 exhibits hydrogen bonding with GLU692 and LYS613 at close distances (2.34 and 2.70 Å, respectively), supported by π-π interactions with PHE612 and TYR670, as well as σ-π and CH-π interactions involving PRO689, ILE760, and LEU750. Similarly, compound 12 forms a hydrogen bond with LYS636 (2.66 Å) and engages in π-π stacking with TYR670 and PHE612. Additional interactions include σ-π bonding with ILE760 and CH-π interaction with PRO689, LEU750, ILE634, and MET682. These interactions collectively stabilise the protein-compound complexes.

Compound 13 shows strong hydrogen bonding, particularly with the OH group of SER614 (2.11 Å) and LYS636 (2.89 Å), along with a π-anion interaction with ASP761 and a π-π stacking with TYR670. It is also supported by the CH-π interaction with LEU750, ILE634, and LEU616, and σ-π interaction with ILE760. In the binding mode of compound 14, dual hydrogen bonding with LYS613 and a π-sulphur interaction with PHE612 were observed. It also exhibits π-anion bonding to GLU692 and π-π stacking with TYR670, further supported by CH-π contacts.

Compound 18 maintains hydrogen bonding with SER614 and LYS636, π-π stacking with TYR670, and σ-π interactions with ILE760. Additional CH-π interactions with ILE634, MET682, LEU750, ILE685, and PRO689 highlight their extensive hydrophobic contacts. Lastly, compound 30 features halogen bonding involving fluorine with GLN683 and PHE684, and hydrogen bonding with ILE685 and SER687 at short distances (1.98 and 2.94 Å, respectively). It also displays π-π stacking with TYR670 and multiple hydrophobic interactions via σ-π and CH-π contacts involving PHE758, ILE634, LEU750, MET682, and PRO689.

The analysis also shows that TYR670 and PHE612 are the most frequently engaged residues, often participating in π-π stacking interactions, and ILE634, LEU750, and MET682 appear consistently across compounds as key contributors to hydrophobic interactions (CH-π and σ-π). On the polar interaction front, LYS613 and LYS636 are commonly involved in hydrogen bonding. SER614 amino acid also emerges as a critical hydrogen-bond donor/acceptor, particularly with compounds featuring hydroxyl or polar moieties. In addition, GLU692 is notable for forming both hydrogen bonds and π-anion interactions.

On the other hand, the sulfonamide NH group frequently forms hydrogen bonds with key polar residues such as LYS613, LYS636, SER614, and GLU692. At the same time, sulfonyl oxygens may participate in electrostatic or π-anion interactions, especially with residues like GLU692 or ASP761, contributing to binding orientation and specificity. Beyond polar interactions, the sulfonamide core also introduces a degree of lipophilicity and structural rigidity, allowing it to support hydrophobic contacts (e.g., CH-π interactions) with residues like ILE634, LEU750, and MET682, particularly when substituted with aromatic or alkyl groups.

It is important to note that all compounds in the top group interact with amino acids such as PHE612, ILE634, TYR670, LEU750, TLE760, and LYS636. These residues are key components of the protein's active site, as reported in previous studies [11, 28].

3.4. In silico prediction of pharmacokinetic properties, toxicity, and drug-likeness

The six compounds with the strongest interactions with the Vps34 enzyme were subjected to further theoretical investigation for their pharmacokinetic properties, toxicity, and drug-likeness.

Lipinski's Rule of Five: a set of guidelines used in drug discovery to evaluate the drug-likeness based on the five criteria, including molecular mass, lipophilicity (XLOGP3 [35], hydrogen-bond donors-acceptors, and molar refractivity. These five criteria help predict good oral bioavailability by ensuring the compound is not too large or overly hydrophilic-lipophilic, which affects its absorption, distribution, metabolism, and excretion (ADME) properties. Typically, a compound with no more than one violation of these rules is considered drug-like and has a higher chance of success as an orally administered medication [36, 37] (Table 2).

Table 2. Prediction of key molecular descriptors in accordance with Lipinski's Rule of Five.

Compound	8	12	13	14	18	30
Molecular mass	403.5	406.5	404.4	378.4	424.4	409.4
Lipophilicity (XLOGP3)	3.54	3.30	4.25	3.45	3.92	3.50
Hydrogen bond donors	1	2	2	1	1	0
Hydrogen bond acceptors	4	4	5	5	7	6
Molar refractivity	111.5	113.5	110.8	102.8	107.9	110.9
No. of violation	0	0	0	0	0	0
Drug-likeness (Lipinski)	Yes	Yes	Yes	Yes	Yes	Yes

All six compounds (8, 12, 13, 14, 18, and 30) satisfy Lipinski's Rule of Five, suggesting they have good potential for oral bioavailability. Their molecular masses are all below 500 Da, which supports favourable absorption. The lipophilicity values (LogP) are well below the threshold of 5, indicating a balanced hydrophilic-lipophilic profile beneficial for permeability. All compounds have fewer than five hydrogen-bond donors and fewer than 10 hydrogen-bond acceptors, fulfilling important criteria for drug-likeness. Additionally, the molar refractivity values for each compound fall within the recommended 40-130 range, reflecting suitable molecular size and polarisability. The strict compliance with Lipinski's Rule of Five indicates they are likely good candidates for further drug development focused on oral administration.

Bioavailability radar: To evaluate the oral bioavailability potential of the selected six compounds, radar plots summarising key physicochemical properties - lipophilicity (LIPO), molecular size (SIZE), polarity (POLAR), insolubility (INSOLU), unsaturation (INSATU), and molecular flexibility (FLEX) - were analysed. The SwissADME "bioavailability radar" of the six compounds are presented in Fig. 9.

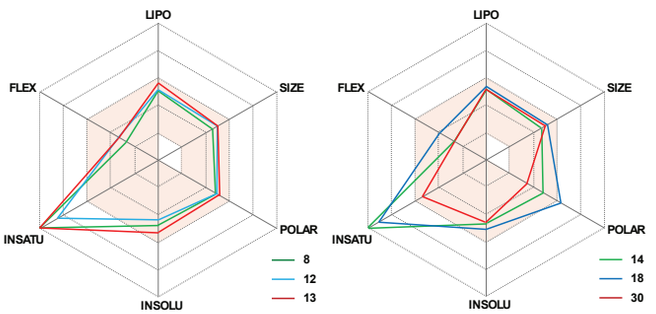

Fig. 9. Bioavailability radar of the six compounds. The light salmon shade indicates the suitable physicochemical space for the oral bioavailability*.

The SwissADME "bioavailability radar" analysis indicates that all six sulfonamide derivatives (8, 12, 13, 14, 18, 30) reside largely within the optimal physicochemical space for oral drugs. Lipophilicity (LogP≈3-4), molecular weight/size (350-450 g/mol), polarity (TPSA~80-90 Å^2), and flexibility (≤6 rotatable bonds), each fall inside or touch the desirable pink zone, suggesting efficient passive permeation across gastrointestinal membranes. Solubility is only mildly limiting, while unsaturation (low fraction sp^3) is the sole descriptor consistently outside the optimal range, reflecting the series' flat, aromatic scaffolds. Among the set, compound 30 displays the most balanced profiles, fully satisfying every radar criterion except unsaturation and therefore emerges as a promising candidate for further study. Overall, the radar plots support good oral bioavailability potential for the series, with only modest structural optimisation required to improve the unsaturation properties.

ADME and toxicity properties: Deep-PK predictions of ADME pharmacokinetic properties, and toxicity of the compounds are listed in Table 3. The data show low to moderate Caco-2 permeability logP_{app} (-5.14 to -4.84) for all compounds, with compound 18 showing the lowest permeability and compound 30 exhibiting the highest. Oral bioavailability was predicted at medium confidence for most compounds, except compound 30, which had high confidence, suggesting its oral drug potential. All compounds showed high-confidence intestinal absorption, suggesting favourable uptake despite permeability differences. All compounds showed generally low skin permeability. These findings align with SwissADME and Lipinski analyses, confirming good oral absorption potential for most compounds except 18, which may need optimisation. Overall, compound 30

*(LIPO (Lipophilicity) -0.7<XLOGP3<+5.0; SIZE (Molecular Size) 150 g/mol<MW<500 g/mol; POLAR (Polarity) 20 Å²<TPSA<130 Å²; INSOLU (Insolubility) -6<Log S (ESOL)<0; INSATU (Unsaturation) 0.25< Fraction Csp3<1; FLEX (Flexibility) 0<Number of rotatable bonds 9).

is prioritised for further study, with compounds 13 and 18 showing potential for alternate delivery routes (Table 3).

Table 3. Deep-PK predictions of absorption, distribution, metabolism, and excretion and toxicity properties of the compounds.

Properties absorption	8	12	13	14	18	30
CaCo-2 permeability ($logP_{app}$)	-5.14	-4.94	-4.95	-4.86	-4.84	-4.92
Human oral bioavailability 20%	Y[a]	Y	Y	Y	Y	YY[aa]
Human intestinal absorption	YY	YY	YY	YY	YY	YY
Skin permeability (cm/h)	-1.98	-3.20	-2.37	-1.92	-1.37	-4.43
Distribution						
Blood-brain barrier (logBB)	-2.07	-2.50	-2.77	-2.24	-3.14	-2.85
Metabolism						
Inhibitor of breast cancer resistance protein	YY	YY	YY	YY	YY	Y
CYP1A2 inhibitor	Y	N	Y	YY	YY	N
CYP2C19 inhibitor	YY	Y	YY	YY	Y	YY
CYP2C9 inhibitor	YY	YY	YY	YY	Y	Y
CYP2D6 inhibitor	N	YY	YY	N	N	N
CYP3A4 inhibitor	Y	Y	Y	Y	Y	YY
Excretion						
Clearance (ml/min/kg)	1.89	-0.07	-0.95	0.36	2.62	3.60
Organic cation transporter 2	N	N	N	N	N	N
Half-life of drug	<3 h	<3 h	<3 h	<3 h	<3 h	<3 h
Toxicity						
Ames mutagenesis; biodegradation; carcinogenesis	Safe	Safe	Safe	Safe	Safe	Safe
Avian	Safe	Safe	Safe	Safe	Toxic	Safe
Bee	Safe	Safe	Safe	Safe	Safe	Toxic
Crustacean	Toxic	Toxic	Safe	Safe	Toxic	Safe
Liver injury I/II	Toxic	Toxic	Toxic	Toxic	Toxic	Toxic
Eye corrosion and eye irritation	Safe	Safe	Safe	Safe	Safe	Safe
Maximum tolerated dose (mg/kg/day)	0.56	0.84	0.53	0.46	0.85	0.23
hERG blocker	Safe	Safe	Safe	Safe	Safe	Safe
Skin sensitisation	Toxic	Safe	Safe	Safe	Safe	Safe
Skin Sensitisation	Toxic	Safe	Safe	Safe	Safe	Safe

Y: Active with medium or low confidence; YY: Active with high confidence; N: inactive.

All six analogues are predicted to inhibit the BCRP efflux transporter and multiple enzymes of the cytochrome P450 superfamily of enzymes, albeit with distinct isozyme-specific profiles. Notably, all compounds show inhibition of CYP2C19, CYP2C9, and CYP3A4 (mostly with high confidence, although compound 8 only weakly inhibits CYP3A4), whereas CYP1A2 and CYP2D6 inhibition is more selective. Compounds 14 and 18 are high-confidence CYP1A2 inhibitors while 12 and 30 are predicted non-inhibitors of CYP1A2 (with 8 and 13 showing moderate inhibition), and only compounds 12 and 13 act as high-confidence inhibitors of CYP2D6, with the remaining analogues showing no significant CYP2D6 inhibition. These contrasting high-confidence inhibition patterns suggest that compounds 12 and 13 may pose higher metabolic instability and drug-drug interaction risks by potently blocking multiple CYP pathways (including CYP2D6), potentially slowing the clearance of co-administered drugs or the compounds themselves. In contrast, compounds lacking inhibition of certain CYPs (for example, no CYP2D6 inhibition for 8, 14, 18, and 30; no CYP1A2 inhibition for 12 and 30) could be metabolised via those routes without interference, implying a more favourable clearance and DDI profile via those specific pathways. Nevertheless, the universal BCRP inhibition and prevalent CYP3A4 inhibition across this series underscore a need for caution regarding transporter-and CYP-mediated pharmacokinetic interactions in their further development.

All derivatives are predicted to be non-inhibitors of OCT2 and to clear rapidly ($t_{½}$<3 h), with compound 30 showing the highest modelled clearance and compounds 12-13 the lowest. Toxicology screens flag no Ames mutagenicity, carcinogenicity, eye irritation, or hERG inhibition liability, but all six carry a liver-injury alert that deserves *in vitro* validation. Compound 8 shows skin sensitisation potential, whereas ecotoxicity is compound-specific (crustacean toxicity for 8, 12, 18; avian for 18; bee for 30). Overall, the series displays manageable systemic clearance and generally acceptable safety, but hepatotoxic and environmental liabilities should be prioritised during lead optimisation.

3.5. Molecular dynamic simulations

The results clearly demonstrate that compound 30 represents the most balanced lead, exhibiting strong inhibitory activity, favourable ADME characteristics, and minimal metabolic liabilities. Therefore, MD simulations were performed to gain deeper insights into the interactions between compound 30 and the target protein. The simulations were conducted for 200 ns under NPT ensemble conditions, maintaining a temperature of 300 K and a pressure of 1.01325 atm, with an energy cutoff of 1.2 kcal/mol. Trajectories were recorded at 100 ps intervals throughout the simulation.

Root Mean Square Deviation analysis: The RMSD profiles of the protein, ligand, and protein-ligand complex are shown in Fig. 10. The RMSD of the protein increased rapidly during the first 20 ns, reflecting initial structural relaxation and adaptation to the simulation environment. Following this phase, the protein RMSD stabilised at approximately 0.28 nm, indicating that the backbone conformation reached equilibrium and remained stable throughout the 200 ns trajectory. The absence of any significant long-term drift suggests that the protein preserved its native structural integrity without undergoing major conformational rearrangements.

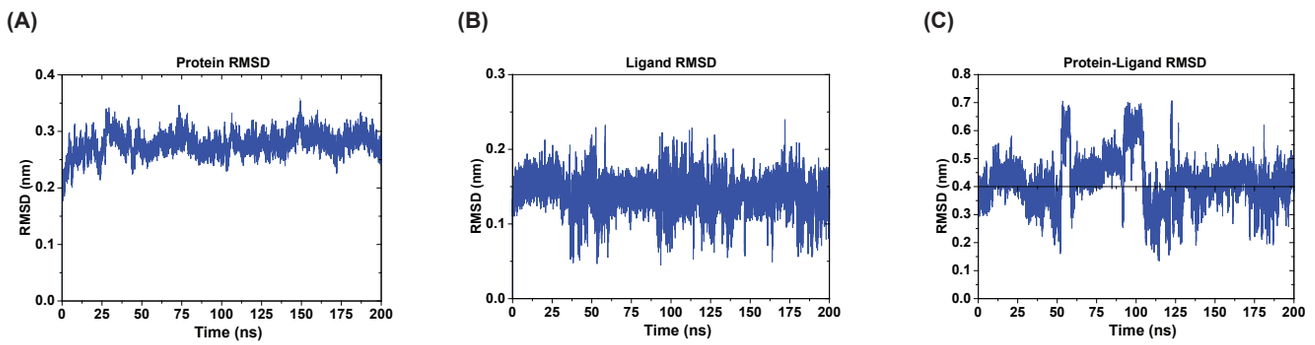

Fig. 10. Graphs showing the trajectories of root mean square deviation (RMSD) of the (A) protein; (B) ligand; (C) protein-ligand complex over the 200 ns simulation period.

In contrast, the ligand exhibited consistently low RMSD values (~0.15 nm) across the entire simulation, indicating a highly stable conformation and strong anchoring within the binding pocket, with only minor internal flexibility. Similarly, the RMSD of the protein-ligand complex showed moderate fluctuations during the initial 120 ns, then stabilised around 0.4 nm after approximately 150 ns, signifying the establishment of a stable binding pose. Overall, these results confirm that the ligand remained securely bound within the protein pocket, forming a well-equilibrated complex.

Root Mean Square Fluctuation analysis: The residue-wise RMSF profile is illustrated in Fig. 11. The plot reveals generally low flexibility (<0.2 nm) across most residues, indicating overall structural stability of the protein. Distinct peaks reaching approximately 0.6 nm were observed between residues 350-500, corresponding to flexible loop regions or surface-exposed segments located near the binding site. These localised fluctuations may contribute to ligand accommodation and binding adaptability, while the rest of the protein remains largely rigid and stable throughout the simulation.

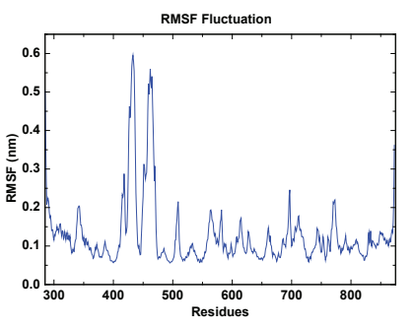

Fig. 11. Residue-wise root mean square fluctuation profile.

Radius of Gyration (Rg): The Rg is a measure of the compactness of a protein structure - lower values indicate a more compact structure, while higher values suggest a more expanded or flexible conformation. The plot illustrates the Rg over a simulation period for compound 30 and the protein. It is clearly shown in Fig. 12 that the radius of gyration fluctuated narrowly between 2.61 and 2.70 nm, with an average of approximately 2.65 nm, confirming that the protein maintained a compact tertiary structure. The absence of major deviations suggests structural stability and no unfolding throughout the simulation.

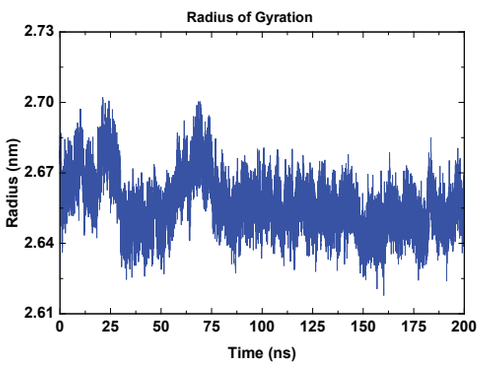

Fig. 12. Radius of gyration of the protein-ligand complex.

Solvent Accessible Surface Area analysis (SASA): The total SASA fluctuated slightly around 285-295 nm^2, indicating a stable degree of solvent exposure. The consistent SASA values reflect the preservation of protein compactness and confirm that no significant conformational expansion occurred during the simulation (Fig. 13).

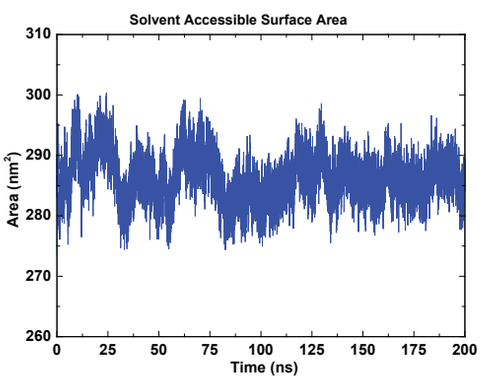

Fig. 13. Plot showing solvent accessible surface area of the protein-ligand complex.

Hydrogen bonding: The hydrogen bond profile between compound 30 and the target protein was monitored throughout the 200 ns simulation, and the result is presented in Fig. 14. The complex consistently maintained 2-4 hydrogen bonds during the trajectory, indicating stable and persistent interactions that contribute significantly to the overall binding affinity. The sustained hydrogen bonding network further supports the structural stability observed in RMSD and Rg analyses, highlighting the strong and specific recognition between compound 30 and the active site residues.

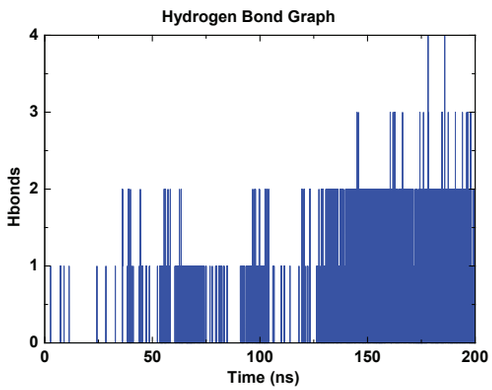

Fig. 14. Graph showing number of hydrogen bonds between compound 30 and the protein.

4. Conclusions

This theoretical investigation highlights the potential of N-heterocycle-containing sulfonamide derivatives as selective inhibitors of the cancer-related Vps34 enzyme. Molecular docking identified six compounds - 8, 12, 13, 14, 18, and 30 - with strong binding affinities (>8.5 kcal/mol) and favourable interactions with key active site residues, such as PHE612, ILE634, TYR670, LEU750, TLE760, and LYS636, indicating their potential inhibition activity. These candidates also demonstrated compliance with drug-likeness criteria and showed promising oral bioavailability profiles. Compound 30 emerged as the most balanced lead, combining potent inhibition, favourable ADME properties, and minimal metabolic liabilities. *In silico* ADMET analysis further supported their pharmacokinetic viability, although liver toxicity and ecotoxicity alerts. Further molecular dynamic simulation also demonstrate that compound 30 can form a stable and well-equilibrated complex with the target protein, maintaining structural integrity, compactness, and consistent binding interactions throughout the 200 ns trajectory. These results support further experimental efforts towards sulfonamide-based compounds, especially 30, as Vps34 inhibitors for cancer treatment.

CRediT author statement

Man Nguyen An Khanh, Le Minh Duc: Methodology, Investigation; Dang Thanh Tuan, Pham Anh Son, Do Huy Hoang: Data analysis, Manuscript draft preparation; Nguyen Van Ha: Literature, Conceptualisation, Data analysis, Supervision, Reviewing and Final editing.

ACKNOWLEDGEMENTS

This research was funded by the research project QG.23.76 of Vietnam National University, Hanoi.

COMPETING INTERESTS

The authors declare that there is no conflict of interest regarding the publication of this article.

REFERENCES

[1] J.M. Backer (2008), "The regulation and function of class III PI3Ks: Novel roles for Vps34", *Biochem. J.*, **410(1)**, pp.1-17, DOI: 10.1042/BJ20071427.

[2] X. Jiang, Y. Bao, H. Liu, et al. (2017), "Vps34 stimulation of p62 phosphorylation for cancer progression", *Oncogene*, **36(50)**, pp.6850-6862, DOI: 10.1038/onc.2017.295.

[3] Q. Wu, D. Zhou, Z. Shen, et al. (2023), "VPS34-IN1 induces apoptosis of ER+ breast cancer cells via activating PERK/ATF4/CHOP pathway", *Biochem. Pharmacol.*, **214**, DOI: 10.1016/j.bcp.2023.115634.

[4] N. Jaber, W.X. Zong (2013), "Class III PI3K Vps34: Essential roles in autophagy, endocytosis, and heart and liver function", *Ann. N. Y. Acad. Sci.*, **1280**, pp.48-51, DOI: 10.1111/nyas.12026.

[5] M.Z. Noman, S. Parpal, K.V. Moer, et al. (2020), "Inhibition of Vps34 reprograms cold into hot inflamed tumors and improves anti-PD-1/PD-L1 immunotherapy", *Sci. Adv.*, **6(18)**, DOI: 10.1126/sciadv.aax7881.

[6] D.X. Hu, S. Patel, H. Chen, et al. (2022), "Structure-based design of potent, selective, and orally bioavailable VPS34 kinase inhibitors", *J. Med. Chem.*, **65(17)**, pp.11500-11512, DOI: 10.1021/acs.jmedchem.1c01180.

[7] A. Ovung, J. Bhattacharyya (2021), "Sulfonamide drugs: Structure, antibacterial property, toxicity, and biophysical interactions", *Biophys. Rev.*, **13(2)**, pp.259-272, DOI: 10.1007/s12551-021-00795-9.

[8] K.A. Elsayad, G.F. Elmasry, S.T. Mahmoud, et al. (2024), "Sulfonamides as anticancer agents: A brief review on sulfonamide derivatives as inhibitors of various proteins overexpressed in cancer", *Bioorg. Chem.*, **147**, DOI: 10.1016/j.bioorg.2024.107409.

[9] J. Lv, J. Zhang, J. Cai, et al. (2024), "Design, synthesis and mechanism study of coumarin-sulfonamide derivatives as carbonic anhydrase IX inhibitors with anticancer activity", *Chem. Biol. Interact.*, **393**, DOI: 10.1016/j.cbi.2024.110947.

[10] L. Rubab, S. Afroz, S. Ahmad, et al. (2022), "An update on synthesis of coumarin sulfonamides as enzyme inhibitors and anticancer agents", *Molecules*, **27(5)**, DOI: 10.3390/molecules27051604.

[11] B. Pasquier, Y. El-Ahmad, B. Filoche-Rommé, et al. (2015), "Discovery of (2S)-8-[(3R)-3-methylmorpholin-4-yl]-1-(3-methyl-2-oxobutyl)-2-(trifluoromethyl)-3,4-dihydro-2H-pyrimido[1,2-a] pyrimidin-6-one: A novel potent and selective inhibitor of Vps34 for the treatment of solid tumors", *J. Med. Chem.*, **58(1)**, pp.376-400, DOI: 10.1021/jm5013352.

[12] C. Colovos, T.O. Yeates (1993), "Verification of protein structures: Patterns of nonbonded atomic interactions", *Protein Sci.*, **2(9)**, pp.1511-1519, DOI: 10.1002/pro.5560020916.

[13] D. Eisenberg, R. Lüthy, J.U. Bowie (1997), "VERIFY3D: Assessment of protein models with three-dimensional profiles", *Methods Enzymol.*, **277**, pp.396-404, DOI: 10.1016/S0076-6879(97)77022-8.

[14] R.A. Laskowski, M.W. MacArthur, D.S. Moss, et al. (1993), "PROCHECK: A program to check the stereochemical quality of protein structures", *J. Appl. Crystallogr.*, **26(2)**, pp.283-291, DOI: 10.1107/S0021889892009944.

[15] R.A. Laskowski, J. Jabłońska, L. Pravda, et al. (2018), "PDBsum: Structural summaries of PDB entries", *Protein Sci.*, **27(1)**, pp.129-134, DOI: 10.1002/pro.3289.

[16] A.M. Waterhouse, G. Studer, X. Robin, et al. (2024), "The structure assessment web server: For proteins, complexes and more", *Nucleic Acids Res.*, **52(W1)**, pp.W318-W323, DOI: 10.1093/nar/gkae270.

[17] C.J. Williams, J.J. Headd, N.W. Moriarty, et al. (2018), "MolProbity: More and better reference data for improved all-atom structure validation", *Protein Sci.*, **27(1)**, pp.293-315, DOI: 10.1002/pro.3330.

[18] Dassault Systèmes BIOVIA (2019), *Discovery Studio Visualizer*, San Diego.

[19] L. Jaillet, S. Artemova, S. Redon (2017), "IM-UFF: Extending the universal force field for interactive molecular modeling", *J. Mol. Graph. Model.*, **77**, pp.350-362, DOI: 10.1016/j.jmgm.2017.08.023.

[20] A. Daina, O. Michielin, V. Zoete (2017), "SwissADME: A free web tool to evaluate pharmacokinetics, drug-likeness and medicinal chemistry friendliness of small molecules", *Sci. Rep.*, **7**, DOI: 10.1038/srep42717.

[21] T.I. Adelusi, A.Q.K. Oyedele, I.D. Boyenle, et al. (2022), "Molecular modeling in drug discovery", *Inform. Med. Unlocked*, **29**, DOI: 10.1016/j.imu.2022.100880.

[22] M. Rudrapal, W.A. Eltayeb, G. Rakshit, et al. (2023), "Dual synergistic inhibition of COX and LOX by potential chemicals from Indian daily spices investigated through detailed computational studies", *Sci. Rep.*, **13(1)**, DOI: 10.1038/s41598-023-35161-0.

[23] F.A.D.M. Opo, M.M. Rahman, F. Ahammad, et al. (2021), "Structure based pharmacophore modeling, virtual screening, molecular docking and ADMET approaches for identification of natural anti-cancer agents targeting XIAP protein", *Sci. Rep.*, **11(1)**, DOI: 10.1038/s41598-021-83626-x.

[24] Y. Myung, A.G.C. De Sá, D.B. Ascher (2024), "Deep-PK: Deep learning for small molecule pharmacokinetic and toxicity prediction", *Nucleic Acids Res.*, **52(W1)**, pp.W469-W475, DOI: 10.1093/nar/gkae254.

[25] S. Seal, M. Mahale, M. García-Ortegón, et al. (2025), "Machine learning for toxicity prediction using chemical structures: Pillars for success in the real world", *Chem. Res. Toxicol.*, **38(5)**, pp.759-807, DOI: 10.1021/acs.chemrestox.5c00033.

[26] O. Aly, R.H. Mekky, F. Pereira, et al. (2024), "Deciphering the potential of *Cymbopogon citratus* (DC.) Stapf as an anti-obesity agent: Phytochemical profiling, *in vivo* evaluations and molecular docking studies", *Food & Function*, **15(24)**, pp.12146-12168, DOI: 10.1039/d4fo04602a.

[27] P. Bauer, B. Hess, E. Lindahl (2022), *GROMACS 2022 Manual*, 669pp, DOI: 10.5281/zenodo.6103568.

[28] M.S. Vaedes-Tresanco, M.E.V. Tresanco, M.R. Carrasquilla, et al. (2021), "Tailored parameterization of the LIE method for calculating the binding free energy of Vps34-inhibitor complexes", *ACS Omega*, **6(44)**, pp.29525-29536, DOI: 10.1021/acsomega.1c03582.

[29] K.E. Hevener, W. Zhao, D.M. Ball, et al. (2009), "Validation of molecular docking programs for virtual screening against dihydropteroate synthase", *J. Chem. Inf. Model.*, **49(2)**, pp.444-460, DOI: 10.1021/ci800293n.

[30] H.A. Odhar, A.F. Hashim, S.W. Ahjel, et al. (2023), "Molecular docking and dynamics simulation analysis of the human FXIIa with compounds from the Mcule database", *Bioinform.*, **19(2)**, pp.160-166, DOI: 10.6026/97320630019160.

[31] H. Lafridi, F.A. Almalki, T.B. Hadda, et al. (2023), "In silico evaluation of molecular interactions between macrocyclic inhibitors with the HCV NS3 protease: Docking and identification of antiviral pharmacophore site", *J. Biomol. Struct. Dyn.*, **41(6)**, pp.2260-2273, DOI: 10.1080/07391102.2022.2029571.

[32] M.V. Kachaeva, D.M. Hodyna, I.V. Semenyuta, et al. (2018), "Design, synthesis and evaluation of novel sulfonamides as potential anticancer agents", *Comput. Biol. Chem.*, **74**, pp.294-303, DOI: 10.1016/j.compbiolchem.2018.04.006.

[33] A. El-Mekabaty, H.M. Awad (2020), "Convenient synthesis of novel sulfonamide derivatives as promising anticancer agents", *J. Heterocycl. Chem.*, **57(3)**, pp.1123-1132, DOI: 10.1002/jhet.3849.

[34] K.J. Okolotowicz, M. Dwyer, D. Ryan, et al. (2018), "Novel tertiary sulfonamides as potent anti-cancer agents", *Bioorg. Med. Chem.*, **26(15)**, pp.4441-4451, DOI: 10.1016/j.bmc.2018.07.042.

[35] T. Cheng, Y. Zhao, X. Li, et al. (2007), "Computation of octanol–water partition coefficients by guiding an additive model with knowledge", *J. Chem. Inf. Model.*, **47(6)**, pp.2140-2148, DOI: 10.1021/ci700257y.

[36] C.A. Lipinski (2004), "Lead- and drug-like compounds: The rule-of-five revolution", *Drug Discov. Today Technol.*, **1(4)**, pp.337-341, DOI: 10.1016/j.ddtec.2004.11.007.

[37] B. Jayaram, T. Singh, G. Mukherjee, et al. (2012), "Sanjeevini: A freely accessible web-server for target directed lead molecule discovery", *BMC Bioinform.*, **13**, DOI: 10.1186/1471-2105-13-S17-S7.